HIGH-ORDER FINITE-VOLUME WEIGHTED ESSENTIALLY NON-OSCILLATORY WENO-$\theta 6$ METHOD FOR THE UNSTEADY EULER EQUATIONS IN ONE-DIMENSIONAL COMPUTATIONAL FLUID DYNAMICS SIMULATIONS

Nguyen Minh Hieu Pham, Thien Binh Nguyen*

Computational Engineering Study Program, Vietnamese-German University, Vietnam

*Corresponding author: binh.nt@vgu.edu.vn

(Received: April 14, 2025; Revised: June 16, 2025; Accepted: June 18, 2025)

DOI: 10.31130/ud-jst.2025.23(6A).211E

Abstract - A sixth-order finite-volume WENO method is proposed for one-dimensional problems with shocks in computational fluid dynamics simulations in which the hyperbolic Euler system are the governing equations. Finite-volume spatial discretization is a natural approach for hyperbolic problems, thanks to its conservation property. Adaptively switching between high-order and low-order reconstructed solutions at the finite-volume cell interfaces using a new set of symmetric smoothness indicators, the developed method excels in resolving small-scaled structures in smooth regions of the solution and sharply capturing shocks and discontinuities without introducing non-physical oscillatory disturbances in the numerical approximation in the vicinity of shocks. Numerical comparisons with other latest WENO methods demonstrate the outperformance of our proposed method.

Key words - WENO-$\theta 6$; Finite Volume Method; Euler equations; hyperbolic conservation laws; computational fluid dynamics

1. Introduction

Wave propagation and convective phenomena play an essential role in numerical modelling and simulation with numerous applications in fluid dynamics, meteorology, astrophysics, and electromagnetism, among others [1-9]. The underlying governing equations are hyperbolic partial differential equations (PDEs). Notable examples include the Euler equations, the magnetohydrodynamic (MHD) equations, and the Maxwell equations. Hyperbolic PDEs are well known for their highly nonlinear property, which accepts discontinuities, e.g., shocks and contacts, to co-exist and develop in time alongside smooth regions in the solution, even though a smooth initial configuration is supplemented. This poses immense challenges in developing a solving strategy, both analytically and numerically.

A numerical approximation method that works for a hyperbolic system must be able to prevent spurious oscillations from developing in the vicinity of shock regions. Early developed strategy was the Total Variation Diminishing (TVD) method in which the total variation of the numerical scheme was kept under control in an exchange of accuracy loss, especially near extrema [10], [11]. To improve the accuracy, Essentially Non-Oscillatory (ENO) [12-13], and later on, Weighted ENO (WENO) [14] were developed. For all ENO-family schemes, the fundamental design principle involves a nonlinear convex combination of reconstruction stencils. This approach adaptively chooses the stencil that provides the highest possible accuracy for solution reconstruction while preventing additional oscillations in the numerical approximation, particularly in shock regions. Prominent WENO schemes include WENO-JS [15 - 18], mapped WENO [19], and WENO-Z [20 - 21] for fifth-order methods, and WENO-NW6 [22 - 23], WENO-CU6 [24], or the recently developed WENO-Z6 [25], WENO6-S [26] or WENO-CZ6 [27] for sixth-order methods.

In this work, we propose the implementation of the sixth-order WENO-$\theta 6$ scheme in the framework of finite volume spatial discretization for the one-dimensional Euler system. WENO-$\theta 6$ was initially developed in a finite difference approach for hyperbolic problems [2]. An extension of the scheme to finite volume substantially enhances the applicability of the method to computational fluid dynamics simulations in which the conservation laws are naturally satisfied and more options are valid regarding meshing techniques to tackle problems with complicated computational domains. By adaptively switching between an upwind and a central reconstruction stencil combined with the choice of a new set of symmetric smoothness indicators, the WENO-$\theta 6$ scheme excels in both resolving shocks and discontinuities without introducing oscillations and maintaining a high-order solution approximation in smooth regions.

2. Finite-Volume WENO Methods for the Euler Equations

2.1. Governing Equations

The Euler equations form a system of conservation laws including the conservation of mass, conservation of momentum, and conservation of energy. In the one-dimensional setting, the Euler equations are written as follows.

$$\begin{cases} \frac{\partial \rho}{\partial t} + \frac{\partial (\rho u)}{\partial x} = 0, \\ \frac{\partial (\rho u)}{\partial t} + \frac{\partial (\rho u^2 + p)}{\partial x} = 0, \\ \frac{\partial E}{\partial t} + \frac{\partial (u(E+p))}{\partial x} = 0. \end{cases} \quad (1)$$

Here, $\rho(x,t)$ represents the fluid density, u the velocity, E the total energy per unit volume, and p the pressure. For an ideal gas, the pressure is related to the conserved variables via the equation of state:

$$p = (\gamma - 1)\left(E - \frac{1}{2}\rho u^2\right), \quad (2)$$

where γ is the ratio of specific heats, typically 1.4 for air [1].

Owing to their hyperbolicity, the system (Euler) can be written in a conserved form of

$$\frac{\partial U}{\partial t} + \frac{\partial F(U)}{\partial x} = 0, \quad (3)$$

where U is the vector of conserved variables and $F(U)$ is the analytical flux function. Explicitly, we have that

$$U = \begin{pmatrix} \rho \\ \rho u \\ E \end{pmatrix}, F(U) = \begin{pmatrix} \rho u \\ \rho u^2 + p \\ u(E+p) \end{pmatrix}. \quad (4)$$

The Euler equations are pivotal in modeling a wide range of physical phenomena in fluid dynamics, particularly in scenarios where viscous effects can be neglected. They underpin many numerical simulations in computational fluid dynamics (CFD), where they are employed to capture shock waves, supersonic flows, and complex interactions in aerodynamics. Moreover, these equations serve as a foundational tool in astrophysics for simulating stellar phenomena, such as supernova explosions and accretion processes, as well as in engineering applications like nozzle flow analysis and the design of high-speed propulsion systems [28].

2.2. Finite Volume Spatial Discretization

The finite-volume method (FVM) discretizes the Euler equations by approximating cell average $I_i = \left[x_{i-\frac{1}{2}}, x_{i+\frac{1}{2}}\right]$

$$U_i(t) \approx \frac{1}{\Delta x}\int_{x_{i-\frac{1}{2}}}^{x_{i+\frac{1}{2}}} U(x,t)dx, \quad (5)$$

And evolving in time via a flux difference

$$\frac{dU_i}{dt} = -\frac{1}{\Delta x}\left(\hat{F}_{i+\frac{1}{2}} - \hat{F}_{i-\frac{1}{2}}\right). \quad (6)$$

Here, the numerical flux

$$\hat{F}_{i+\frac{1}{2}} = \hat{F}\left(\tilde{U}_i^R, \tilde{U}_{i+1}^L\right), \quad (7)$$

replaces the analytical one to approximate the flux amount through both cell interfaces. Here, $\tilde{U}_i^R$ and $\tilde{U}_{i+1}^L$ are the reconstructed values of the solution on the left and right side of the interface $x_{i+\frac{1}{2}}$ taken from the two adjacent cells I_i and I_{i+1}, respectively, sharing the interface $x_{i+\frac{1}{2}}$. Conditions of a good choice of a numerical flux are well established and can be found in [29-30]. For this work, the global Lax-Friedrichs numerical flux is implemented throughout all numerical tests, which is given below, [31],

$$\hat{F}_{i+\frac{1}{2}} = \frac{1}{2}\left[f\left(\tilde{U}_i^R\right) + f\left(\tilde{U}_{i+1}^L\right)\right] - \frac{\alpha}{2}\left(\tilde{U}_{i+1}^L - \tilde{U}_i^R\right), \quad (8)$$

with

$$\alpha = \max_{U}(|f'(U)|), \quad (9)$$

And f is the analytical fluxes.

2.3. Time Discretization

Spatial discretization of the Euler equations in FVM yields a semi-discrete ordinary-discrete equations (ODE) system for cell averages,

$$\frac{dU_i}{dt} = \hat{L}(U_i), \quad (10)$$

where,

$$\hat{L}(U_i) := -\frac{1}{\Delta x}\left(\hat{F}_{i+\frac{1}{2}} - \hat{F}_{i-\frac{1}{2}}\right). \quad (11)$$

In our work, we couple the sixth-order finite-volume $\theta 6$ spatial discretization method with a third-order strong-stability preserving Runge-Kutta time-stepping method (SSP RK3) to maintain stability in time, which is given below, [32],

$$U^{(1)} = U^n + \Delta t \cdot \hat{L}(U^n), \quad (12)$$

$$U^{(2)} = \frac{3}{4}U^n + \frac{1}{4}U^{(1)} + \frac{1}{4}\Delta t \cdot \hat{L}\left(U^{(1)}\right), \quad (13)$$

$$U^{n+1} = \frac{1}{3}U^n + \frac{2}{3}U^{(1)} + \frac{2}{3}\Delta t \cdot \hat{L}\left(U^{(2)}\right). \quad (14)$$

3. Sixth-Order Finite-Volume WENO-$\theta 6$ Method for the Euler Equations

The WENO-$\theta 6$ scheme was initially proposed by Jung and Nguyen in the context of finite-difference spatial discretization [2]. WENO-$\theta 6$ scheme adaptively switches between a 5th-order upwind and a 6th-order central reconstruction based on the local smoothness of the solution, thereby improving the scheme's accuracy and stability. The developed finite-difference WENO-$\theta 6$ increases the accuracy order to a sixth order when compared with conventional fifth-order WENO-JS [15] or WENO-Z [20-21] schemes, which results in a significant improvement in resolving small-scaled structures present in smooth regions of the solution. In addition, by an adaptive selection between an upwind and a central stencil for the reconstruction procedure, WENO-$\theta 6$ mitigates the drawback in maintaining solution symmetry of other sixth-order WENO methods, i.e. WENO-NW6 [22] and WENO-CU6 [24].

In this section, we develop the WENO-$\theta 6$ scheme in the setting of finite-volume discretization. We note that finite volume is derived based on the principle of analytical preservation of conservation laws. In this regard, the finite-volume WENO-$\theta 6$ scheme, possessing all the good properties of its finite-difference counterpart, is more natural and beneficial for computational fluid dynamics simulations, in which the inviscid Euler equations and the viscous Navier-Stokes equations play a main role as governing equations. We note that, unlike finite difference where the flux is approximated at grid points, it is the solution $\tilde{U}$ itself that is reconstructed over cells via the WENO procedure in finite volume.

3.1. WENO Schemes

Finite-volume WENO schemes achieve a high-order accuracy of the reconstructed solution at a cell interface via a nonlinear convex combination of low-order reconstructed solution values. For a scheme of order $2r-1$, the high-order reconstructed $\tilde{U}_{i+\frac{1}{2}}$ on the right interface of cell I_i is calculated by

$$\tilde{U}_{i+\frac{1}{2}} = \sum_{k=0}^{r-1} \omega_k \tilde{U}_{i+\frac{1}{2}}^k; \quad (15)$$

here, r is the number of sub-stencils on which each of the

low-order $\widetilde{U}^k_{i+\frac{1}{2}}$ is reconstructed. For a fifth-order WENO scheme, these $\widetilde{U}^k_{i+\frac{1}{2}}$ are given explicitly as follows,

$$\widetilde{U}^0_{i+\frac{1}{2}} = \frac{2}{6}U_{i-2} - \frac{7}{6}U_{i-1} + \frac{11}{6}U_i, \quad (16)$$

$$\widetilde{U}^1_{i+\frac{1}{2}} = -\frac{1}{6}U_{i-1} + \frac{5}{6}U_i + \frac{2}{6}U_{i+1}, \quad (17)$$

$$\widetilde{U}^2_{i+\frac{1}{2}} = \frac{2}{6}U_i + \frac{5}{6}U_{i+1} - \frac{1}{6}U_{i+2}. \quad (18)$$

The nonlinear weight ω_k is computed for each sub-stencil based on the smoothness indicator of that sub-stencil. The objectives of the nonlinear weights are two-fold: to converge to the linear weights d_k to achieve the optimal accuracy order and essentially eliminate the sub-stencils containing shocks out of the reconstruction procedure. The computation of the nonlinear weights differs from scheme to scheme. For example, in the fifth-order WENO scheme developed by Jiang and Shu [15], the smoothness indicators for the sub-stencils are calculated below,

$$\beta_0 = \frac{13}{12}(U_{i-2} - 2U_{i-1} + U_i)^2 + \frac{1}{4}(U_{i-2} - 4U_{i-1} + 3U_i)^2, \quad (19)$$

$$\beta_1 = \frac{13}{12}(U_{i-1} - 2U_i + U_{i+1})^2 + \frac{1}{4}(U_{i+1} - U_{i-1})^2, \quad (20)$$

$$\beta_2 = \frac{13}{12}(U_i - 2U_{i+1} + U_{i+2})^2 + \frac{1}{4}(3U_i - 4U_{i+1} + U_{i+1})^2, \quad (21)$$

Then, the nonlinear weights are

$$\omega_k = \frac{\alpha_k}{\sum_{j=0}^{r-1}\alpha_j}, \alpha_k = \frac{d_k}{(\beta_k+\epsilon)^p}, \quad (22)$$

with d_k being the linear weights,

$$d_0 = \frac{3}{10}, d_1 = \frac{6}{10}, d_2 = \frac{1}{10}. \quad (23)$$

$\epsilon = 10^{-6}$ and $p = 2$ are tuning parameters to enhance the scheme's sensitivity to smoothness.

3.2. Adaptive Reconstruction

The sixth-order linear reconstruction is defined as

$$\widetilde{U}_{i+\frac{1}{2}} = \sum_{k=0}^{3}\gamma_k^\theta \widetilde{U}^k_{i+\frac{1}{2}}, \quad (24)$$

with weights

$$\gamma_0^\theta = \frac{1}{20}(1+\theta), \gamma_1^\theta = \frac{3}{20}(3+\theta), \quad (25)$$

$$\gamma_2^\theta = \frac{3}{20}(3-\theta), \gamma_3^\theta = \frac{1}{20}(1-\theta). \quad (26)$$

Here, $\widetilde{U}^k_{i+\frac{1}{2}}$ for $k = 0, 1, 2$ are in [12] and

$$\widetilde{U}^3_{i+\frac{1}{2}} = \frac{11}{6}U_{i+\frac{1}{2}} - \frac{7}{6}U_{i+2} + \frac{2}{6}U_{i+3}. \quad (27)$$

The scheme selects between the 5th-order reconstruction $\widetilde{U}^5_{i+\frac{1}{2}}$ (when $\theta = 0$) and the 6th-order one $\widetilde{U}^6_{i+\frac{1}{2}}$ otherwise. Nonlinear weights are computed via

$$\omega_k^\theta = \frac{\alpha_k^\theta}{\sum_{l=0}^{3}\alpha_l^\theta}, \quad (28)$$

$$\alpha_k^\theta = \gamma_k^\theta\left(1 + \frac{\tau^\theta}{\epsilon + \tilde{\beta}_k}\right), \quad (29)$$

where $\tilde{\beta}_k$ is a new set of smoothness indicators for the sub-stencils, $\tilde{\tau}^\theta$ is the large-stencil smoothness indicator, and $\epsilon = 10^{-10}$.

3.3. Symmetric Smoothness Indicators

Standard 6th-order schemes often face issues with asymmetric smoothness indicators, especially for the downwind stencil, WENO-θ6 resolves this by constructing symmetric indicators $\tilde{\beta}_k$, particularly redefining $\tilde{\beta}_3$ over an extended sub-stencil, thereby stabilizing the nonlinear weights and improving performance in transition regions. Detailed expressions for $\tilde{\beta}_k$ are provided in [2]. For $k = 0, 1, 2$, $\tilde{\beta}_k$ are as

$$\tilde{\beta}_0 = \frac{13}{12}(U_{i-2} - 2U_{i-1} + U_i)^2 + (U_{i-2} - 3U_{i-1} + 2U_i)^2, \quad (30)$$

$$\tilde{\beta}_1 = \frac{13}{12}(U_{i-1} - 2U_i + U_{i+1})^2 + (U_{i+1} - U_i)^2, \quad (31)$$

$$\tilde{\beta}_2 = \frac{13}{12}(U_i - 2U_{i+1} + U_{i+2})^2 + (U_i - U_{i+1})^2, \quad (32)$$

and

$$\tilde{\beta}_3 = \frac{13}{48}(3U_i - 7U_{i+1} + 5U_{i+2} - U_{i+3})^2 + \frac{1}{144}(-11U_i + 9U_{i+1} + 3U_{i+2} - U_{i+3})^2, \quad (33)$$

3.4. Large Stencil Smoothness Indicator and Adaptive Selection

Two smoothness indicators, τ_5 and τ_6, are defined by

$$\tau_5 = \frac{13}{12}(U_{i-2} - 4U_{i-1} + 6U_i - 4U_{i+1} + U_{i+2})^2 + (-U_{i-1} + 3U_i - 3U_{i+1} + U_{i+2})^2, \quad (34)$$

$$\tau_6 = \frac{13}{12}(-U_{i-2} + 5U_{i-1} - 10U_i + 10U_{i+1} - 5U_{i+2} + U_{i+3})^2 + \frac{1}{4}(U_{i-2} - 3U_{i-1} + 2U_i - 3U_{i+2} + U_{i+3})^2. \quad (35)$$

The adaptive mechanism selects the smoothness indicators and the corresponding reconstructions via

$$(\tau^\theta, \theta) = \begin{cases}(\tau_6, 0), if\ \tau_6 < \tau_5,\\ (\tau_5, 1), otherwise.\end{cases} \quad (36)$$

This strategy ensures that the scheme achieves 6th-order accuracy in smooth regions (when τ_6 is dominant) and resorts to a more dissipative 5th-order upwind reconstruction near discontinuities, thereby enhancing robustness in complex flow regimes.

4. Numerical Results

4.1. Comparing WENO methods

In our numerical experiments, we compare the performance in terms of accuracy and stability of our proposed finite-volume WENO-θ6 scheme with latest developed WENO schemes. These include the WENO-Z6 [25], WENO6-S [26], and WENO-CZ6 [27].

4.1.1. WENO-Z6

Introduced by Hu [25], the WENO-Z6 scheme extends the framework of the fifth-order WENO-Z method with an

adaptive measure for enhanced stability and efficiency. The global smoothness indicator is computed as follows.

$$\tau = \left|\beta_3 - \frac{1}{6}(\beta_0 + 4\beta_1 + \beta_2)\right| \quad (37)$$

4.1.2. WENO6-S

Huang et al. proposed the sixth-order WENO6-S scheme [26]. The scheme uses a simplified global smoothness indicator to blend reconstructions and reduce dissipation, which is calculated below.

$$\begin{cases} \beta_6 = \frac{R}{R+1/R}\beta_3 + \frac{1/R}{R+1/R}\beta_S, R = \frac{\beta_3+\epsilon}{\beta_S+\epsilon} \\ \beta_S = \frac{Q}{Q+1/Q}\beta_0 + \frac{1/Q}{Q+1/Q}\beta_2, Q = \frac{\beta_0+\epsilon}{\beta_2+\epsilon} \end{cases} \quad (38)$$

4.1.3. WENO-CZ6

Zhao's WENO-CZ6 [27] combines local and global stencil evaluations through adaptive weighting to improve robustness near discontinuities. The global smoothness indicator is defined by

$$\beta_6 = \left(1 + \frac{2\tau}{1+\tau}\right)\frac{\beta_0+\beta_3}{2} \quad (39)$$

4.2. Numerical Tests for Accuracy

4.2.1. Test 1: Linear Advection Equation

We solve

$$\begin{cases} u_t + u_x = 0, x \in (-1,1), \\ u(x,0) = \sin(\pi x), \end{cases} \quad (40)$$

up to time $t = 1.0$ with periodic boundary conditions. The error is measured using the L^1 and L^∞ norms:

$$\left||E|\right|_{L^1} = \Delta x \sum_j \left|u_j^e - \tilde{u}_j\right|, \quad (41)$$

$$\left||E|\right|_{L^\infty} = \max_j \left|u_j^e - \tilde{u}_j\right| \quad (42)$$

and the time step is chosen as $\Delta t = \Delta x^{\frac{6}{3}}$ to isolate spatial discretization errors. As shown in Table 1, all schemes – including WENO-$\theta 6$, WENO-Z6, WENO6-S, and WENO-CZ6 – exhibit 6th-order convergence.

Table 1. *Convergence with initial condition (40): $u(x,0) = sin(\pi x)$. Final time $t = 1.0$. N is the FV control volume number*

Method	N	20	40	80	160	320
WENO-$\theta 6$	L^1 Error	2.7E-5	4.3E-7	6.8E-9	1.0E-10	1.6E-12
	Order	-	5.962	6.993	5.997	6.000
	L^∞ Error	2.1E-5	3.4E-7	5.3E-9	8.3E-11	1.3E-12
	Order	-	5.970	5.991	5.998	5.987
WENO-Z6	L^1 Error	3.3E-5	4.3E-7	6.8E-9	1.0E-10	1.6E-12
	Order	-	6.268	6.000	5.997	6.000
	L^∞ Error	2.6E-5	3.3E-7	5.3E-9	8.3E-11	1.3E-12
	Order	-	6.303	5.977	5.998	5.987
WENO6-S	L^1 Error	3.0E-5	4.3E-7	6.8E-9	1.0E-10	1.6E-12
	Order	-	6.153	5.993	5.998	6.000
	L^∞ Error	3.9E-5	3.4E-7	5.3E-9	8.3E-11	1.3E-12
	Order	-	6.830	6.013	5.999	5.988
WENO-CZ6	L^1 Error	2.7E-5	4.3E-7	6.8E-9	1.0E-10	1.6E-12
	Order	-	5.981	5.994	5.997	6.001
	L^∞ Error	2.1E-5	3.4E-7	5.3E-9	8.3E-11	1.3E-12
	Order	-	5.975	5.991	5.998	5.9839

4.2.2. Test 2: Smooth Euler Equations

Two smooth test cases for the Euler equations are considered on $x \in (0,2)$ with periodic boundaries and final time $t = 2.0$. The first test uses

$$(\rho, u, p) = (1 + 0.2\sin\pi x, 1.0, 1.0). \quad (43)$$

While, the second case employs a modified density profile,

$$(\rho, u, p) = \left(1 + 0.2\left[\sin\pi x - \frac{\sin\pi x}{\pi}\right], 1.0, 1.0\right). \quad (44)$$

Error measurement (see Tables 2 and 3) confirm that all schemes achieve 6th-order accuracy. Notably, WENO-$\theta 6$ consistently produces competitive errors and robust performance, in agreement with previous studies (e.g. [2]).

Table 2. *Convergence with initial condition (43): $(\rho, u, p) = (1 + 0.2\,sin\,\pi x, 1.0, 1.0)$. Final time $t = 2.0$. N is the FV control volume number*

Method	N	20	40	80	160	320
WENO-$\theta 6$	L^1 Error	1.0E-5	1.7E-7	2.7E-9	4.2E-11	6.0E-13
	Order	-	5.964	5.997	5.998	5.8249
	L^∞ Error	8.5E-6	1.3E-7	2.1E-9	3.4E-11	4.3E-13
	Order	-	5.971	5.990	5.969	5.972
WENO-Z6	L^1 Error	1.5E-5	1.7E-7	2.7E-9	4.2E-11	6.0E-13
	Order	-	6.463	5.996	5.998	5.823
	L^∞ Error	1.3E-5	1.3E-7	2.1E-9	3.4E-11	4.4E-13
	Order	-	6.618	6.025	5.964	5.949
WENO6-S	L^1 Error	2.2E-5	1.7E-7	2.7E-9	4.2E-11	6.0E-13
	Order	-	7.017	5.996	5.999	5.825
	L^∞ Error	2.4E-5	1.4E-7	2.1E-9	3.4E-11	4.3E-13
	Order	-	7.387	6.061	5.972	5.961
WENO-CZ6	L^1 Error	1.1E-5	1.7E-7	2.7E-9	4.2E-11	6.0E-13
	Order	-	5.995	5.995	5.998	5.882
	L^∞ Error	8.3E-6	1.3E-7	2.1E-9	3.4E-11	4.4E-13
	Order	-	5.938	5.991	5.968	5.954

Table 3. *Convergence with initial condition (44): $(\rho, u, p) = \left(1 + 0.2\left[sin\,\pi x - \frac{sin\,\pi x}{\pi}\right], 1.0, 1.0\right)$. Final time $t = 2.0$. N is the FV control volume number*

Method	N	20	40	80	160	320
WENO-$\theta 6$	L^1 Error	3.4E-4	4.8E-6	7.8E-8	1.2E-9	2.1E-11
	Order	-	6.179	5.942	5.990	5.863
	L^∞ Error	5.0E-4	7.7E-6	1.2E-7	2.0E-9	3.5E-11
	Order	-	6.023	5.915	5.978	5.841
WENO-Z6	L^1 Error	4.9E-4	4.8E-6	7.8E-8	1.2E-9	2.1E-11
	Order	-	6.683	5.940	5.989	5.863
	L^∞ Error	6.1E-4	7.8E-6	1.2E-7	2.0E-9	3.5E-11
	Order	-	6.298	5.936	5.984	5.844
WENO6-S	L^1 Error	4.3E-4	6.4E-6	9.8E-8	1.4E-9	2.5E-11
	Order	-	6.061	6.026	6.054	5.887
	L^∞ Error	4.9E-4	1.1E-5	2.7E-7	5.2E-9	1.1E-10
	Order	-	5.423	5.405	5.676	5.575
WENO-CZ6	L^1 Error	2.7E-4	4.7E-6	7.8E-8	1.2E-9	2.1E-11
	Order	-	5.839	5.938	5.990	5.863
	L^∞ Error	4.0E-4	7.7E-6	1.2E-7	2.0E-9	3.5E-11
	Order	-	5.698	5.920	5.977	5.841

4.3. Numerical Tests for Stability

4.3.1. Test 3: Wave Package for Linear Scalar Case

This test assesses numerical schemes' ability to resolve smooth and discontinuous features using an initial condition combining a Gaussian, square wave, triangle, and semi-ellipse [15]

$$u(x,0) = \begin{cases} \frac{1}{6}A(x,\beta,z,\delta), x \in [-0.8,-0.6], \\ 1, x \in [-0.4,-0.2], \\ 1-|10(x-0.1)|, x \in [0,0.2], \\ \frac{1}{6}B(x,\alpha,a,\delta), x \in [0.4,0.6], \\ 0, otherwise, \end{cases} \quad (45)$$

where,

$$A(x,\beta,z,\delta) = G(x,\beta,z-\delta) + 4G(x,\beta,z) + G(x,\beta,z+\delta), \quad (46)$$

$$B(x,\alpha,a,\delta) = F(x,\alpha,a-\delta) + 4F(x,\alpha,a) + F(x,\alpha,a+\delta), \quad (47)$$

and

$$G(x,\beta,z) = \exp(-\beta(x-z)^2), \quad (48)$$

$$F(x,\alpha,a) = \sqrt{\max(1-\alpha^2(x-a)^2,0)}. \quad (49)$$

The constants are

$$z = -0.7, \delta = 0.005, \beta = \frac{\log 2}{36\,\delta^2}, \quad (50)$$

$$a = 0.5, \alpha = 10. \quad (51)$$

The numerical results are computed at time $t = 6.3$, with $N = 400$, and periodic boundary conditions. The results of WENO-$\theta 6$ excels in all critical regions, whereas other schemes show oscillations in Figures 2-3.

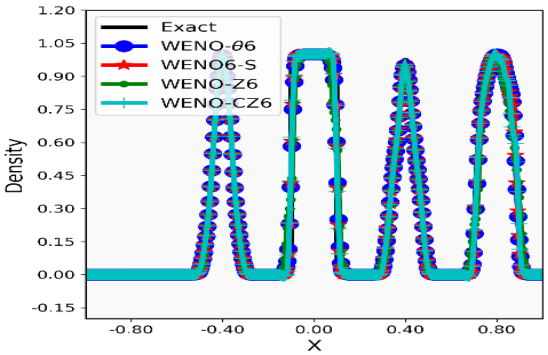

Figure 1. *Stability test with initial condition (45), at final time t = 6.3, and with grid N = 400*

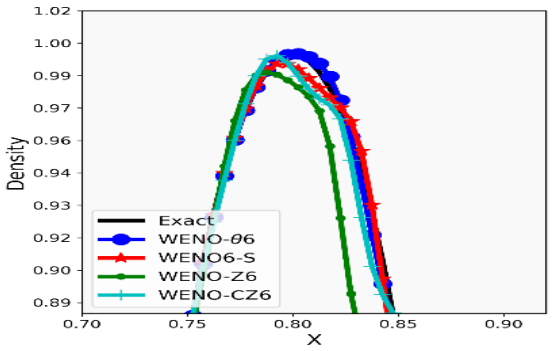

Figure 2. *Stability test with initial condition (45), zoom near the semi-ellipse region*

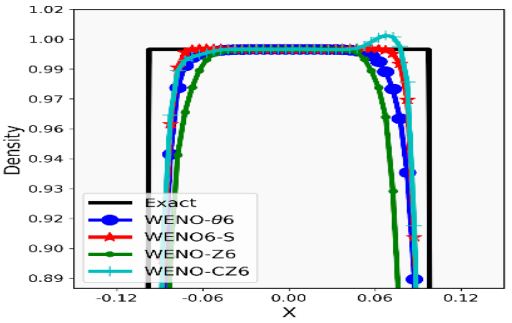

Figure 3. *Stability test with initial condition (45), zoom near the square region*

4.3.2. Test 4: Riemann Problems for the Euler Equations

Riemann's problems, such as Sod's and Lax's cases, test the resolution of discontinuities in hyperbolic conservation laws [1].

- **Sod's problem:**

$$(\rho,u,p) = \begin{cases} (0.125,0,0.1), -5 < x < 0, \\ (1,0,1), 0 < x < 5; \end{cases} \quad (52)$$

with final time $t = 1.7$.

- **Lax's problem:**

$$(\rho,u,p) = \begin{cases} (0.445,0.698,3.528), -5 < x < 0, \\ (0.5,0,0.571), 0 < x < 5; \end{cases} \quad (53)$$

with final time $t = 1.3$.

Further information about the exact solutions to these problems can be found in [33]. All WENO schemes handle Sod's problem well, Figure 4, but in Lax's problem, WENO6-S and WENO-CZ6 exhibit oscillations near contact discontinuities, Figures 5 and 6. WENO-$\theta 6$ and WENO-Z6 demonstrate superior accuracy and stability, with WENO-$\theta 6$ standing out.

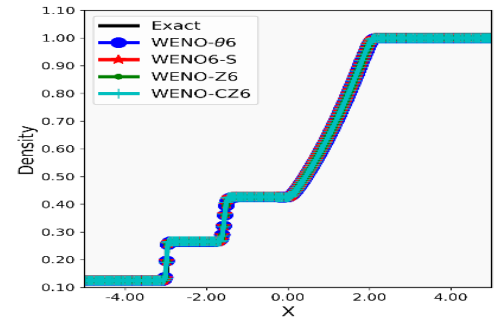

Figure 4. *Stability test for Sod's problem initial condition (52), at time t = 1.7, and with grid N = 300*

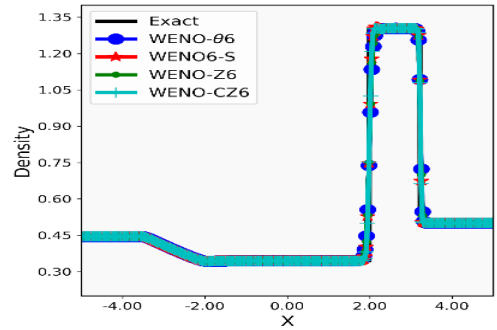

Figure 5. *Stability test for Lax's problem initial condition (53), at final time t = 1.3, and with grid N = 300*

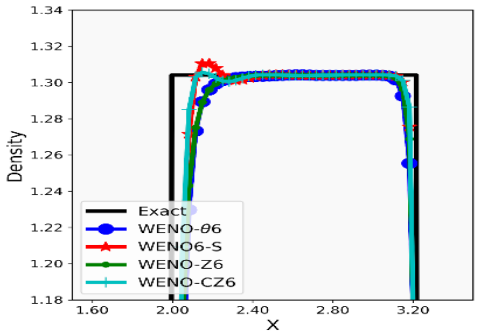

Figure 6. *Stability test for Lax's problem initial condition (53), zoom near the discontinuous region*

4.3.3. Test 5: Shock Density Wave Interaction

The Shu-Osher test [30] evaluates schemes' ability to capture a Mach 3 shock interacting with a sinusoidal density perturbation,

$$(\rho,u,p)=\begin{cases}\left(3.857143,2.629369,\frac{31}{3}\right),-5<x<-4,\\(1+0.2\sin 5x,0,1),-4<x<5;\end{cases} \quad (54)$$

All WENO schemes resolve key features, but WENO-$\theta 6$ offers superior accuracy in specific regions, maintaining stability and robustness throughout the test, Figures 7-8.

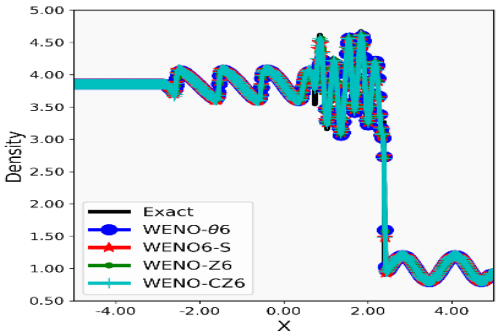

Figure 7. *Stability test for Shu-Osher's problem initial condition (54), at final time t = 1.8, and with grid N = 400*

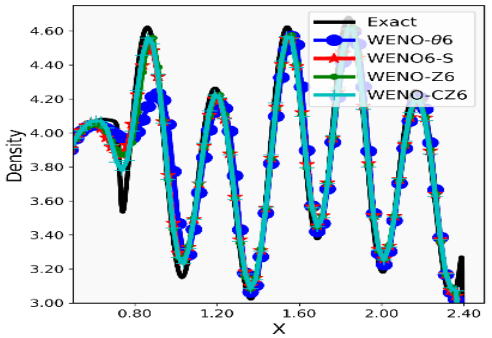

Figure 8. *Stability test for Shu-Osher's problem initial condition (54), zoom near the discontinuous region*

4.3.4. Test 6: Two Interacting Blast Waves

This test [34] examines the interaction of two strong blast waves,

$$(\rho,u,p)=\begin{cases}(1,0,1000),0<x<0.1,\\(1,0,0.01),0.1<x<0.9,\\(1,0,100),0.9<x<1.\end{cases} \quad (55)$$

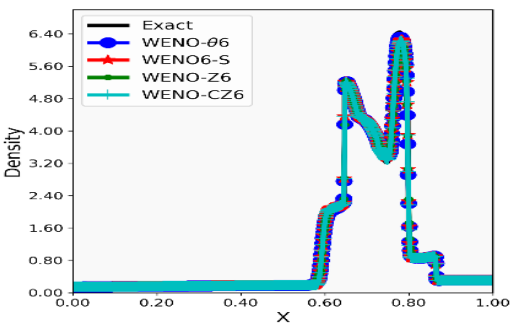

Figure 9. *Stability test for the blast waves problem initial condition (55), at final time t = 0.03, and with grid N = 801*

All WENO schemes perform effectively, with WENO-CZ6 providing the sharpest resolution and WENO-$\theta 6$ following closely, showcasing notable accuracy and efficiency under extreme conditions, Figures 9-10.

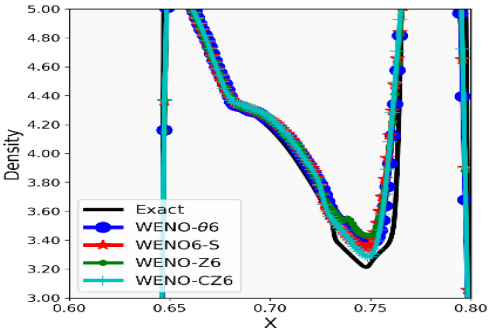

Figure 10. *Stability test for the blast waves problem initial condition (55), zoom near the discontinuous region*

5. Conclusion

This study evaluates the WENO-$\theta 6$ scheme within the finite volume framework, testing its accuracy, robustness, and efficiency against WENO6-S, WENO-Z6, and WENO-CZ6 in numerical experiments like linear wave problems, Euler equations, Riemann problems, and interacting blast waves. WENO-$\theta 6$ proves robust, achieving 6th-order accuracy for smooth solutions and effectively resolving shocks, rarefactions, and contact discontinuities. It outperforms WENO6-S in dissipation and rivals WENO-Z6 in accuracy for Riemann and shock-density wave tests while matching WENO-CZ6 in complex cases like interacting blast waves.

Future work will refine these aspects, extending WENO-$\theta 6$ to two-dimensional systems and engineering problems like supersonic flows and combustion dynamics. With targeted enhancements, WENO-$\theta 6$ can become a more powerful tool for computational fluid dynamics and real-world challenges.

Acknowledgments: This work was funded by the Vietnamese Ministry of Education and Training under grant number B2024-VGU-06.

REFERENCES

[1] E. F. Toro, *Riemann solvers and numerical methods for fluid dynamics: a practical introduction, 3rd ed*. Dordrecht New York: Springer, 2009.

[2] C.-Y. Jung and T. B. Nguyen, "A new adaptive weighted essentially

non-oscillatory WENO- θ scheme for hyperbolic conservation laws", *J. Comput. Appl. Math*., vol. 328, pp. 314–339, Jan. 2018, doi: 10.1016/j.cam.2017.07.019.

[3] D. Christodoulou, "The Euler Equations of Compressible Fluid Flow", *Bull. Am. Math. Soc.,* vol. 44, no. 4, pp. 581–602, Jun. 2007, doi: 10.1090/S0273-0979-07-01181-0.

[4] O. Darrigol and U. Frisch, "From Newton's mechanics to Euler's equations", *Phys. Nonlinear Phenom*., vol. 237, no. 14–17, pp. 1855–1869, Aug. 2008, doi: 10.1016/j.physd.2007.08.003.

[5] P. Hopkins, "O-T Vortex Test Page", *Princeton University Department of Astrophysical Sciences.* [Online]. Available: https://www.astro.princeton.edu/~jstone/Athena/tests/orszag-tang/pagesource.html [Accessed: Mar. 07, 2025].

[6] B. Punsly, D. Balsara, J. Kim, and S. Garain, "Riemann solvers and Alfven waves in black hole magnetospheres", *Comput. Astrophys. Cosmol.*, vol. 3, no. 1, p. 5, Sep. 2016, doi: 10.1186/s40668-016-0018-1.

[7] D. P. Hampshire, "A derivation of Maxwell's equations using the Heaviside notation", *Philos. Trans. R. Soc. Math. Phys. Eng. Sci.*, vol. 376, no. 2134, p. 20170447, Dec. 2018, doi: 10.1098/rsta.2017.0447.

[8] National Institute of Standards and Technology, "CODATA Value: speed of light in vacuum". *physics.nist.gov,* [Online]. Available: https://physics.nist.gov/cgi-bin/cuu/Value?c [Accessed: Mar. 07, 2025].

[9] J. D. Jackson, *Classical electrodynamics, 3. ed.,* [Nachdr.]. Hoboken, NY: Wiley, 2009.

[10] A. Harten, "High resolution schemes for hyperbolic conservation laws", *J. Comput. Phys.*, vol. 49, no. 3, pp. 357–393, Mar. 1983, doi: 10.1016/0021-9991(83)90136-5.

[11] A. Harten, "On a Class of High Resolution Total-Variation-Stable Finite-Difference Schemes", *SIAM J. Numer. Anal.*, vol. 21, no. 1, pp. 1–23, Feb. 1984, doi: 10.1137/0721001.

[12] A. Harten and S. Osher, "Uniformly High-Order Accurate Nonoscillatory Schemes. I", *SIAM J. Numer. Anal.,* vol. 24, no. 2, pp. 279–309, 1987.

[13] A. Harten, B. Engquist, S. Osher, and S. R. Chakravarthy, "Uniformly High Order Accurate Essentially Non-oscillatory Schemes, III", *J. Comput. Phys.*, vol. 131, no. 1, pp. 3–47, Feb. 1997, doi: 10.1006/jcph.1996.5632.

[14] X.-D. Liu, S. Osher, and T. Chan, "Weighted Essentially Non-oscillatory Schemes", *J. Comput. Phys.,* vol. 115, no. 1, pp. 200–212, Nov. 1994, doi: 10.1006/jcph.1994.1187.

[15] G.-S. Jiang and C.-W. Shu, "Efficient Implementation of Weighted ENO Schemes", *J. Comput. Phys.,* vol. 126, no. 1, pp. 202–228, Jun. 1996, doi: 10.1006/jcph.1996.0130.

[16] C.-W. Shu, "High-order Finite Difference and Finite Volume WENO Schemes and Discontinuous Galerkin Methods for CFD", *Int. J. Comput. Fluid Dyn*., vol. 17, no. 2, pp. 107–118, Mar. 2003, doi: 10.1080/1061856031000104851.

[17] D. S. Balsara and C.-W. Shu, "Monotonicity Preserving Weighted Essentially Non-oscillatory Schemes with Increasingly High Order of Accuracy", *J. Comput. Phys.,* vol. 160, no. 2, pp. 405–452, May 2000, doi: 10.1006/jcph.2000.6443.

[18] X. Ji and Y. Zheng, "Characteristic decouplings and interactions of rarefaction waves of 2D Euler equations", *J. Math. Anal. Appl.*, vol. 406, no. 1, pp. 4–14, Oct. 2013, doi: 10.1016/j.jmaa.2012.05.035.

[19] A. K. Henrick, T. D. Aslam, and J. M. Powers, "Mapped weighted essentially non-oscillatory schemes: Achieving optimal order near critical points", *J. Comput. Phys.*, vol. 207, no. 2, pp. 542–567, Aug. 2005, doi: 10.1016/j.jcp.2005.01.023.

[20] R. Borges, M. Carmona, B. Costa, and W. S. Don, "An improved weighted essentially non-oscillatory scheme for hyperbolic conservation laws", *J. Comput. Phys*., vol. 227, no. 6, pp. 3191–3211, Mar. 2008, doi: 10.1016/j.jcp.2007.11.038.

[21] M. Castro, B. Costa, and W. S. Don, "High order weighted essentially non-oscillatory WENO-Z schemes for hyperbolic conservation laws", *J. Comput. Phys.*, vol. 230, no. 5, pp. 1766–1792, Mar. 2011, doi: 10.1016/j.jcp.2010.11.028.

[22] N. K. Yamaleev and M. H. Carpenter, "A systematic methodology for constructing high-order energy stable WENO schemes", *J. Comput. Phys*., vol. 228, no. 11, pp. 4248–4272, Jun. 2009, doi: 10.1016/j.jcp.2009.03.002.

[23] M. H. Carpenter, T. C. Fisher, and N. K. Yamaleev, "Boundary Closures for Sixth-Order Energy-Stable Weighted Essentially Non-Oscillatory Finite-Difference Schemes", *in Advances in Applied Mathematics, Modeling, and Computational Science*, vol. 66, R. Melnik and I. S. Kotsireas, Eds., in Fields Institute Communications, vol. 66., Boston, MA: Springer US, 2013, pp. 117–160. doi: 10.1007/978-1-4614-5389-5_6.

[24] X. Y. Hu, Q. Wang, and N. A. Adams, "An adaptive central-upwind weighted essentially non-oscillatory scheme", *J. Comput. Phys.,* vol. 229, no. 23, pp. 8952–8965, Nov. 2010, doi: 10.1016/j.jcp.2010.08.019.

[25] F. Hu, "The 6th-order weighted ENO schemes for hyperbolic conservation laws", *Comput. Fluids,* vol. 174, pp. 34–45, Sep. 2018, doi: 10.1016/j.compfluid.2018.07.008.

[26] C. Huang and L. L. Chen, "A new adaptively central-upwind sixth-order WENO scheme", *J. Comput. Phys.*, vol. 357, pp. 1–15, Mar. 2018, doi: 10.1016/j.jcp.2017.12.032.

[27] K. Zhao, Y. Du, and L. Yuan, "A New Sixth-Order WENO Scheme for Solving Hyperbolic Conservation Laws", *Commun. Appl. Math. Comput.*, vol. 5, no. 1, pp. 3–30, Mar. 2023, doi: 10.1007/s42967-020-00112-3.

[28] J. D. Anderson, *Computational fluid dynamics: the basics with applications, Internat. ed., Reprint*. in McGraw-Hill series in aeronautical and aerospace engineering. New York: McGraw-Hill, 2006.

[29] C.-W. Shu and S. Osher, "Efficient implementation of essentially non-oscillatory shock-capturing schemes", *J. Comput. Phys.,* vol. 77, no. 2, pp. 439–471, Aug. 1988, doi: 10.1016/0021-9991(88)90177-5.

[30] C.-W. Shu and S. Osher, "Efficient implementation of essentially non-oscillatory shock-capturing schemes, II", *J. Comput. Phys.,* vol. 83, no. 1, pp. 32–78, Jul. 1989, doi: 10.1016/0021-9991(89)90222-2.

[31] C.-W. Shu, *"Essentially non-oscillatory and weighted essentially non-oscillatory schemes for hyperbolic conservation laws*", in Advanced Numerical Approximation of Nonlinear Hyperbolic Equations, vol. 1697, A. Quarteroni, Ed., in Lecture Notes in Mathematics, vol. 1697., Berlin, Heidelberg: Springer Berlin Heidelberg, 1998, pp. 325–432. doi: 10.1007/BFb0096355.

[32] B. Cockburn, S.-Y. Lin, and C.-W. Shu, "TVB Runge-Kutta local projection discontinuous Galerkin finite element method for conservation laws III: One-dimensional systems", *J. Comput. Phys.*, vol. 84, no. 1, pp. 90–113, Sep. 1989, doi: 10.1016/0021-9991(89)90183-6.

[33] P. L. Roe, "Approximate Riemann solvers, parameter vectors, and difference schemes", *J. Comput. Phys.*, vol. 43, no. 2, pp. 357–372, Oct. 1981, doi: 10.1016/0021-9991(81)90128-5.

[34] P. Woodward and P. Colella, "The numerical simulation of two-dimensional fluid flow with strong shocks", *J. Comput. Phys.,* vol. 54, no. 1, pp. 115–173, Apr. 1984, doi: 10.1016/0021-9991(84)90142-6.